Micromagnetic Modeling of All Optical Switching

V. Raposo, E. Martínez, A. Hernández, and M. Zazo

Departamento de Física Aplicada, University of Salamanca, Salamanca E-37008, Spain

The control of the magnetization at the microscale by pure optical means is fundamentally interesting and promises faster speeds for data storage devices. Although several experiments have shown that it is possible to locally reverse the magnetization of a ferromagnetic system by means of laser pulses, a completely theoretical description of these All Optical Switching processes is still lacking. Here, we develop an advanced micromagnetic solver that is applied to the numerical study of the All Optical Switching. The solver is based on the Landau-Lifshitz-Bloch equation that governs the dynamics of the magnetization coupled the microscopic three temperatures model, which describes the temporal evolution of the temperatures of the subsystems as caused by laser heating. The helicity-dependent magnetization switching is evaluated by a magneto-optical effective field caused by the Inverse Faraday Effect when a circularly polarized laser is applied to the sample. All the other usual terms of a full micromagnetic model are included (exchange, anisotropy, DMI…). As a test, the model is used to describe the local magnetization switching of thin film samples with high perpendicular anisotropy. The results are in good agreement with available experimental observations.

***Index Terms*—Micromagnetism, All Optical Switching, Landau-Lifshitz-Bloch equation, three temperatures model, Inverse Faraday Effect.**

I. Introduction

Manipulation of magnetism using ultrafast laser pulses without any external magnetic field, also called All Optical Switching (AOS), is fundamentally interesting and promises for low-power and high-speed spintronic devices. Since the discovery of the ultrafast demagnetization of a Nickel film by a femtosecond laser pulse, many experiments have confirmed the manipulation of magnetization by ultrafast laser beams. The earlier experimental works studied ferrimagnetic alloys [1][2][3], followed by synthetic ferrimagnets [4], and more recently, also ferromagnetic materials [5] irradiated with a train of laser pulses resulting in AOS. Several experiments have confirmed the helicity-dependent control of the magnetization by circularly polarized laser pulses, obtaining the magnetization switching of the area under the laser beam [6], the movement of a domain wall [7], and even the nucleation of an inverted domain under the path of a moving laser beam[5][8][4].

Although the helicity-dependent all optical switching (HD-AOS) is well established from an experimental point of view, the theoretical description of these processes is still far to be completely understood, and in particular, there exists several physical phenomena involved which need to be evaluated within a full micromagnetic formalism. The most evident effect is the heating of the sample at femtosecond scale as due to the laser pulses. This effect can be analyzed by the two or three temperatures models [9], which describes the temporal evolution of the temperatures of the constituent subsystems (electrons, phonons and spins). On the other hand, the helicity-dependent switching of the magnetization may be determined by other mechanisms related to the coupling between the circular polarization of the laser pulse and the local magnetization. These helicity-dependent phenomena include the Inverse Faraday Effect (IFE) [10][11][12][13][14], the magnetic circular dichroism (MCD) [15][16][17], or even the laser-induced spin currents [18][19][20][21]. Nowadays it remains unclear which is the role of these mechanisms in a particular AOS experiment. While the physics under the AOS is still under debate, the most established mechanism for HD-AOS in ferromagnetic samples is the induction of a transient demagnetized state caused by the laser heating, followed by the remagnetization of the sample under the magnetic field caused by the IFE. The direction of this magneto-optical effective field is determined by the laser helicity (σ) [1], which favors a given direction for the remagnetized state.

Several approaches to describe the AOS mechanisms have been presented, including the three temperatures model (3TM) coupled to simplified Landau-Lifshitz-Bloch equation (LLB) [22][23][24][25]. However, solving the full micromagnetic problem is a complicated task, as the samples used for AOS are large, with sizes of hundreds of μm^2. The involved time scales in these processes also differ over a wide range, going from the femtosecond scale of the laser pulses, the picosecond scale for temperature evolution, and nanosecond scale for the domain dynamics and temperature dissipation to the substrate. The temperature even exceeds the Curie point of the sample, and consequently LLB eq. must be numerically solved. This requires small time stepping, which makes the numerical problem even much more time consuming. Additionally, special care must be taken when solving the temperatures equations when short pulses with high power are applied. Up to now, there was no full micromagnetic simulator that takes into account all the physics involved in extended samples and provided a realistic description of available HD-AOS experiments.

In this paper we present micromagnetic simulations based on an advanced micromagnetic model that couples the laser heating described by the 3TM to temporal evolution of the magnetization given by the LLB equation. The coupling between the circularly-polarized laser pulses and the magnetization is assumed to be caused by the IFE, which generates a transient helicity-dependent magneto-optical effective field that is able to reproduce the most relevant experimental observation of AOS in ferromagnetic thin-film with high perpendicular magnetic anisotropy (PMA).

II. MICROMAGNETIC MODEL

In a typical AOS experiment, a ferromagnetic layer grown over a substrate is subjected to the action of a laser beam, with a typical duration from hundreds of fs to several ps. The laser spot is assumed to have a space Gaussian profile with a full width at half maximum defined by the radius r_0. The temporal profile of these pulses is assumed to be Gaussian, with τ_L being its full width at half maximum duration. Therefore, the space and temporal profile of the laser power is:

$$P(r,t) = P_0 \exp\left[-\frac{r^2}{r_0^2/(4ln2)}\right]\exp\left[-\frac{(t-t_0)^2}{\tau_L^2/(4ln2)}\right] \quad (1)$$

where $r = \sqrt{x^2+y^2}$ is the distance from the center of the laser spot and t_0 is the time at which the laser power reaches its maximum power (P_0) in the center of the laser spot. The maximum power of the laser is $P_0 = F/(t_{FM}\tau_L)$, where F is the laser fluence, and $t_{FM}$is the thickness of the ferromagnetic sample.

The numerical model developed here takes into account the underlying physics of opto-thermal and opto-magnetic coupling between the laser beam and the ferromagnetic layer. The optical energy provided by the light generates hot carriers in the ferromagnetic layer. The 3TM [23][9] describes the transient temperature response of the system, including electrons, phonons and spins. The spin temperature is introduced in the LLB equation that describes the temporal dependence of the magnetization at temperatures close to or even above the Curie temperature (T_C).

In order to describe the opto-magnetic coupling between the laser and the ferromagnetic layer, here we assume, in agreement with experimental observations, that the IFE is the dominant helicity-dependent effect. It is responsible of a transient out-of-plane magneto-optical effective field ($\vec{B}_{MO} \propto \pm\vec{u}_z$) with an orientation that depends on the helicity ($\sigma^{\pm}$) of the laser beam as will be described after. The evaluation of the local magnetization $\vec{M}(\vec{r},t)$ under these circularly-polarized laser pulses is described by the LLB equation [24] [30]. The optically-induced magnetization dynamics is described by the corresponding LLB equation which is given by [30]:

$$\frac{d\vec{m}(\vec{r},t)}{dt} = -\gamma_0'\vec{m}\times\vec{H}_{eff} - \gamma_0'\frac{\alpha_\perp}{m^2}\left[\vec{m}\times\left(\vec{m}\times\left(\vec{H}_{eff}+\vec{H}_{th}^{\perp}\right)\right)\right] + \gamma_0'\frac{\alpha_\parallel}{m^2}\left(\vec{m}\cdot\vec{H}_{eff}\right)\vec{m} + \vec{H}_{th}^{\parallel} \quad (2)$$

where $\vec{m}(\vec{r},t) = \vec{M}(\vec{r},t)/M_s^0$ is the normalized magnetization with M_s^0 the saturation magnetization at $T=0$, and $m = m(T) \equiv |\vec{m}|$. $\gamma_0' = \gamma_0/(1+\alpha^2)$ with γ_0 being the gyromagnetic ratio and α is the Gilbert damping. $\alpha_\parallel$ and $\alpha_\perp$ are the longitudinal and transverse damping parameters given by:

$$\alpha_\parallel = \alpha\left(\frac{2T}{3T_C}\right) \quad (3)$$

$$\alpha_\perp = \alpha\left(1-\frac{T}{3T_C}\right) \quad (4)$$

where T_C is the Curie temperature. The effective field $\vec{H}_{eff}$ in (1) includes all the conventional interactions of the micromagnetic theoretical framework, and the magneto-optical field due to the IFE ($\vec{H}_{MO}$):

$$\vec{H}_{eff} = \vec{H}_{exch} + \vec{H}_{DM} + \vec{H}_{dmg} + \vec{H}_{ani} + \vec{H}_m + \vec{H}_{MO} \quad (5)$$

where $\vec{H}_{exch}$ is the exchange contribution, $\vec{H}_{DM}$ is the interfacial Dzyaloshinskii-Moriya interaction (DMI), $\vec{H}_{dmg}$ is the demagnetizing field, and $\vec{H}_{ani}$ is the PMA field. $\vec{H}_m$ represents the internal exchange field in the LLB eq, which is given by:

$$\vec{H}_m = \begin{cases} \frac{1}{2\chi_\parallel}\left(1-\frac{m^2}{m_e^2}\right)\vec{m}, & T < T_C \\ -\frac{1}{\chi_\parallel}\left(1+\frac{3}{5}\frac{T_C m^2}{(T-T_C)}\right)\vec{m}, & T > T_C \end{cases} \quad (6)$$

where $\chi_\parallel$ is the longitudinal susceptibility [30],

$$\chi_\parallel = \frac{\partial m_e}{\partial H_{ext}}\Big)_{H_{ext}\to 0} = \frac{\frac{\mu_0\mu_B}{k_B T}B'(x)}{\left(1-\frac{T_C}{T}B'(x)\right)} \quad (7)$$

and $m_e = m_e(T)$ is the equilibrium value of $m = m(T)$. $B'(x) = \frac{\partial B(x)}{\partial x}$ with $B(x)$ being the Brillouin function, k_B the Boltzmann constant, and μ_B the Bohr magneton. Note that at a given instant of time, the local magnetization is not in general in thermal equilibrium. The LLB eq. can evaluate this non-equilibrium physics. Further details of the implementation of the LLB equation are given in [30].

The magneto-optical field ($\vec{B}_{MO}(\vec{r},t) = \mu_0\vec{H}_{MO}(\vec{r},t)$) is the local effective field due to the circular polarization of the laser beam. This out-of-plane field ($\vec{H}_{MO}$) emerges as consequence of the IFE [11][26][27], and it can be expressed as:

$$\vec{B}_{MO}(\vec{r},t) = (\sigma^{\pm})\, F\, \chi_{IFE}\, f_{MO}(\vec{r},t)\vec{u}_z \quad (8)$$

where $\sigma^{\pm} = \pm 1$ is the laser helicity, where each sign correspond to one of the two senses of circular polarization of the laser. F (in [(J/m^2)]) is the laser fluence and χ_{IFE} (in [T/(J/m^2)]) is the IFE susceptibility. Therefore, the maximum value of the magneto-optical field ($B_{max} = F\,\chi_{IFE}$) is achieved when the laser power reaches its maximum value ($t = t_0$) in the center of the laser beam ($r = 0$). The function $f_{MO}(\vec{r},t)$ describes the space-temporal dependence of the magneto-optical field as

$$f_{MO}(\vec{r},t) = \begin{cases} \exp\left[-\frac{r^2}{r_0^2/(4\,ln\,2)}\right]\exp\left[-\frac{(t-t_0)^2}{\tau_L^2/(4\,ln\,2)}\right], & t < t_0 \\ \exp\left[-\frac{r^2}{r_0^2/(4\,ln\,2)}\right]\exp\left[-\frac{(t-t_0)^2}{(\tau_L+\tau_d)^2/(4\,ln\,2)}\right], & t > t_0 \end{cases} \quad (9)$$

where τ_d represents the delay of the magneto-optical field with respect to the laser pulse [23], and in agreement with several experimental observations, it accounts for some persistence of the $\vec{B}_{MO}(\vec{r},t)$ due to the optical laser signal. The value of the χ_{IFE} depends on the sample characteristics, but typical values of the fluence predicts magnitudes of B_{MO} in the range from 1 to 100T [28].

The LLB eq. (2) also includes stochastic terms $\vec{H}_{th}^{\perp}$ and $\vec{H}_{th}^{\parallel}$ to account for stochastic fluctuations due to the thermal noise. The first one ($\vec{H}_{th}^{\perp}$) is a random thermal field orthogonal to the local magnetization, whereas the second one ($\vec{H}_{th}^{\parallel}$) describes the longitudinal noise, parallel to the local magnetization. Their statistical properties are summarized by:

$$\begin{gathered}\langle H_i^{\perp}(t)\rangle = 0 \\ \langle H_i^{\perp}(\vec{r},t)H_j^{\perp}(\vec{r}',t')\rangle = \frac{2K_B T(\alpha_{\perp}-\alpha_{\parallel})}{\gamma_0' M_s^0 V \alpha_{\perp}^2}\delta_{ij}\delta(t-t')\delta(\vec{r}-\vec{r}') \\ \langle H_i^{\parallel}(t)\rangle = 0 \\ \langle H_i^{\parallel}(\vec{r},t)H_j^{\parallel}(\vec{r}',t')\rangle = \frac{2\gamma_0' T\alpha_{\parallel}}{M_s^0 V \alpha_{\perp}^2}\delta_{ij}\delta(t-t')\delta(\vec{r}-\vec{r}') \\ \langle H_i^{\perp}(\vec{r},t)H_j^{\parallel}(\vec{r}',t')\rangle = 0\end{gathered} \tag{10}$$

In these expressions, the notation $\langle\cdots\rangle$ indicates the average over different stochastic realizations of the noise, and the sub-indexes are the Cartesian components, $i,j: x,y,z$. V is the volume of the computational cell (see [30] for more details).

The temperature evolution in the system under the action of the laser pulses is described by the 3TM in terms of three subsystems involving the electron (T_e), the lattice (T_l) and the spin (T_s) temperatures [9]. Note that the relevant temperature for the magnetic system described by previously introduced LLB eq. (2) is the spin temperature, $T_s(\vec{r},t) \equiv T(\vec{r},t)$, but this one depends on the temperature of the electron ($T_e(\vec{r},t)$) and the lattice ($T_l(\vec{r},t)$) subsystems, as given by the following coupled set of differential equations:

$$\begin{cases} C_e\dfrac{\partial T_e}{\partial t} = -k_e\nabla^2 T_e - g_{el}(T_e - T_l) - g_{es}(T_e - T_s) + P(r,t) \\ C_l\dfrac{\partial T_l}{\partial t} = -k_l\nabla^2 T_l - g_{el}(T_l - T_e) - g_{ls}(T_l - T_s) \\ C_s\dfrac{\partial T_s}{\partial t} = -k_s\nabla^2 T_s - g_{es}(T_s - T_e) - g_{ls}(T_s - T_l) \end{cases} \tag{11}$$

where C_i is the thermal capacity (in $[\mathrm{J/(m^3K)}]$) and k_i is the thermal conductivity (in $[\mathrm{W/(m\cdot K)}]$) of each subsystem ($i: e,l,s$). g_{ij} are the coupling constants between subsystems (in $[\mathrm{W/K}]$). $P(r,t)$ is the laser power, which is absorbed by the sample, as given by eq. (1). Note that above Debye temperature, C_l and C_s can be considered as constant parameters, whereas, C_e is linear with the electron's temperature, $C_e = \gamma_e T_e$ where $\gamma_e = \frac{C_e(300\ \mathrm{K})}{300\ \mathrm{K}}$. The influence of the substrate can be also taken into account by adding an additional Newton-like term to the right hand side of the second one of these equations ($-(T - T_{sub})/\tau_{sub}$), where T_{sub} is the substrate temperature, and the τ_{sub} is a characteristic time which describes the heat transport to the substrate and the surrounding [31].

III. Results and Discussion

The implementation of the LLB equation was checked by evaluating the temperature dependence of the magnetization, reproducing the expected behavior. At each temperature, the distribution of the magnetization values was found in perfect accordance to the Boltzmann distribution, giving the same results as presented in [24]. The 3TM also was compared to the numerical resolution of the equations given in (11), obtaining the same results for the finite difference implementation.

For the simulations we adopted the typical thermal and micromagnetic parameters for a Pt/Co bilayer: $M_S^0 = 1.1\ \mathrm{MA/m}$, uniaxial PMA constant $K_u = 1.25\ \mathrm{MJ/m^3}$, $T_C = 550\mathrm{K}$, damping factor $\alpha = 0.5$, exchange stiffness $A_{ex} = 15\ \mathrm{pJ/m}$, DMI constant $D = 2.25\ \mathrm{mJ/m^3}$, $k_e = 91\mathrm{W/(m\cdot K)}$, $C_e(300\mathrm{K}) = 2.8\times10^5\ \mathrm{J/(m^3K)}$, $C_L = 3.7\times10^6\ \mathrm{J/(m^3K)}$, $C_s = 2.8\times10^5\ \mathrm{J/(m^3K)}$, $g_{ij} = 1.5\times10^{18}\ \mathrm{W/m^3}$, $\tau_{sub} = 0.9$ ns. Disorder was taken into account in the form of grains, with a random a variation of the easy-axis direction of the anisotropy $\pm3°$ from grain to grain, being 15 nm the characteristic grain size [32].

Fig. 1 shows some of the laser inputs used to analyze the HD-AOS. In Fig. 1(b) the temporal evolution of the normalized power of the laser beam and the magnitude of the magneto-optical effective field, are plotted at the center of the spot ($r = 0$). As discussed previously, the magneto-optical effective field $\vec{B}_{MO}(\vec{r},t)$ lasts longer than the laser pulse. Fig 1(c) presents the typical time evolution of the temperatures of the three subsystems (electrons T_e, lattice T_l and spins T_s) before, during and after the application of the laser pulse. The effect of the substrate is evidenced in Fig, 1(d) by the long relaxation time of the temperature (τ_{sub}). All the relevant values of these laser and magneto-optical field parameters are given in the caption of Fig. 1.

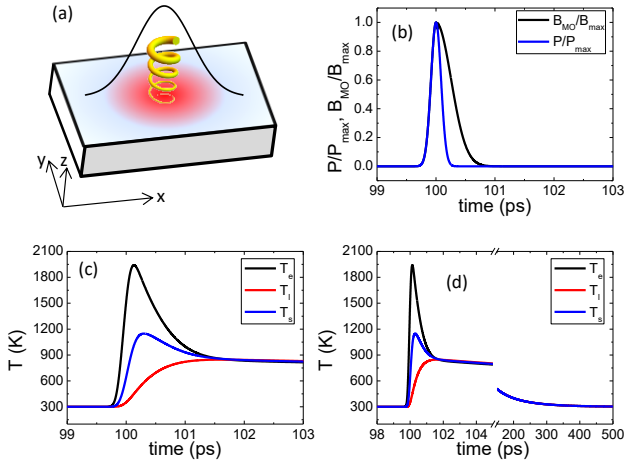

Fig. 1. Schematic view of the system (a) and temporal evolution of the temperatures of the three subsystems (electrons, lattice and spins) in the center of the laser beam as obtained from the 3TM. (b) Temporal evolution of the normalized magneto-optical field (B_{MO}/B_{max}) and the normalized laser power (P/P_{max} where $P_{max} \equiv P_0$) at the center of the laser beam. The laser pulse is

$\tau_L = 200$ fs, the delay of the magneto-optical field is $\tau_d = \tau_L$, and the circularly polarized laser pulse has positive (or right-handed) helicity ($\sigma^+ = +1$). (c) Temporal evolution of the temperature of the three subsystems: electrons (T_e), lattice (T_l) and spins (T_s). These temperatures are plotted here at the center of the laser beam ($r = 0$). (d) Same as in (b) with indication of the relaxation of the three temperatures towards the room value for long times after the laser pulse. The fluence considered here is $F = 6$ J/m^2.

We simulated a Co/Pt thin-film with high PMA of 1.5μm ×1.5μm ×0.8nm submitted to a train of 25 circularly polarized laser pulses with $\tau_L = 200$ fs, $F = 0.55$ J/m^2 and $r_0 = 768$ nm, that induces a maximum magneto-optical effective field of 5T with $\tau_d = 400$ fs. Fig. 2 summarizes the time evolution of the magnetization (out-of-plane component, $m_z(r,t)$), which clearly shows the transient inversion of the magnetization in the region under the influence of the laser pulses as due to the heating. However, the terminal switching is only achieved for a proper combination of the initial state of the magnetization ($m_z(r,0) = \pm 1$) and the polarization of the laser pulses $\sigma^{\pm} = \pm 1$. Indeed, when the helicity ($\sigma^{\pm}$) induces a magneto-optical effective field ($\vec{B}_{MO} \propto (\sigma^{\pm})\vec{u}_z$) in the opposite direction than the initial magnetization (2nd and 3rd rows in Fig. 2), the All Optical Switching is achieved in the illuminated area. Note that the snapshots in the last column of Fig. 2 show the terminal stable magnetic state for a long time after the last laser pulse. On the other hand, when the laser helicity generates an effective field $\vec{B}_{MO}$ in the same direction as the initial magnetic state, the optical switching is not achieved (1st and 4th rows in Fig. 2). Therefore, the IFE can explain the results of the AOS for ferromagnetic samples as combined to the temperature increase due to the laser heating.

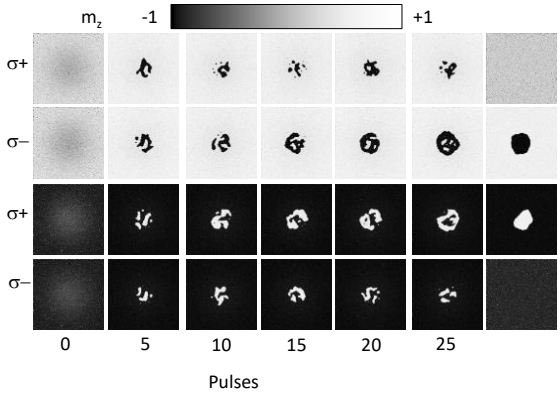

Fig. 2. Snapshots of the temporal evolution out-of-plane magnetization ($m_z(r,t)$) for right (σ^+) and left (σ^-) helicities of the laser beam under the influence of the IFE starting with the magnetization pointing up ($m_z(r,0) = +1$) and down ($m_z(r,0) = -1$). The fluence and the maximum value of the opto-magnetic effective field are $F = 0.55$ J/m^2, $B_{max} = 5$ T respectively. The last column shows the terminal magnetic state after 25 ns from the end of the last laser pulse.

The inversion of the magnetization is only possible when the sample reaches the Curie temperature under the laser beam, where the magneto-optical effective field is present $\vec{B}_{MO}$. This is evidenced in Fig. 3(a), where the inversion is only attained for high enough fluence F. Here, the initial state is the same, pointing up, $m_z(r,0) = +1$, and laser pulses with left-handed helicity (σ^-) are applied with different values of the fluence F. Note that for this helicity ($\sigma^- = -1$), the magneto-optical field $\vec{B}_{MO} \propto (\sigma^{\pm})\vec{u}_z$ promotes the switching to the down state ($\vec{B}_{MO} \propto -\vec{u}_z$), as it was already discussed in Fig. 2. However, the final switching also depends on the laser fluence. At $F = 0.45$ J/m^2 the center of the laser beam reaches 558 K (see Fig. 3(b)), slightly over T_C and it is not able to heat a region that nucleates an inverted domain. However, at higher fluence, $F = 0.55$ J/m^2, the temperature increases up to 603 K and the inversion is achieved (see Fig 3(c), where the reduction of the $< m_z >$ corresponds to the inversion of the central region). The notation $< m_z >$ indicates the average of the out-of-plane magnetization over the whole sample. The switching is also achieved for higher fluences ($F > 0.55$ J/m^2), as the temperature exceeds T_C in a region similar to the size spot of the laser beam. Fig. 3(d) presents the temporal evolution of the averaged m_z at the center of the sample over a circle of 100 nm of radius for $F = 0.45$ J/m^2 and $F = 0.55$ J/m^2. The notation $< m_{z,center} >$ indicates that the average of the out-of-plane magnetization is computed at the center of the sample over a circle of 100 nm of radius. It is clearly observed that after the demagnetization of each pulse the sample recovers the initial state ($< m_{z,center} > \approx -1$) for low fluence $F = 0.45$ J/m^2. However, if the fluence increases to $F = 0.55$ J/m^2, when the number of pulses increases, the centrally averaged magnetization first cancels ($< m_{z,center} > \approx 0$), due to the multi-domain structure, and then collapses to a single domain with negative magnetization ($< m_{z,center} > \approx -1$). Therefore, our results indicates that there is a minimum fluence threshold of about 0.50 J/m^2 to achieve the helicity dependent AOS in the evaluated samples.

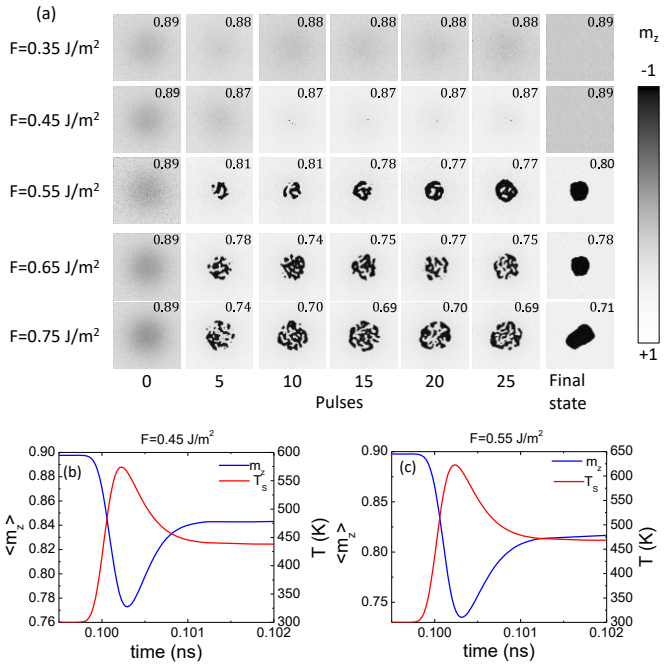

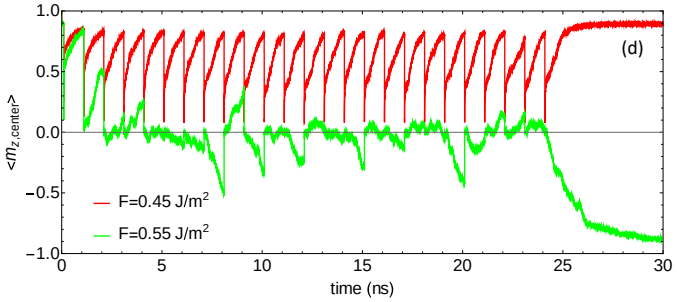

Fig. 3. (a) Snapshots of the out-of-plane magnetization ($m_z(r,t)$) over time for left (σ^-) helicity of the laser beam under the influence of the IFE starting with the magnetization pointing up ($m_z(r,0)=+1$). The maximum magnitude of the $\vec{B}_{MO}$ is $B_{max}=5$ T, and it points along the negative out-of-plane direction for the left-handed helicity (σ^-, $\vec{B}_{MO}\sim-\vec{u}_z$) The number in the top-right of every snapshot indicates the average value of m_z over the whole sample ($<m_z>$). (b) and (c) show the details of the temporal evolution of the average out-of-plane magnetization over the sample volume ($<m_z>$) and the spin temperature ($T\equiv T_s$) at the center of the laser spot for two fluences: under (b) and over (c) the threshold fluence that leads to switching. (d) Temporal evolution of the magnetization averaged over a circular region of radius $r=100$ nm around the center of the sample, $<m_{z,center}>$ for $F=0.45\,J/m^2$ and $F=0.55\,J/m^2$

The snapshots of the magnetization simulated by our model presented in Fig. 2 can explain the experimental results of Fig. 3 in reference [7]. For high enough fluence there is an increase of the inverted region as the number of pulses increases, as shown in Fig. 2 and 3a, and this fact became more evident for the highest fluence. There is an expansion of the inverted region for each pulse and the final reversed area increases. Initially, at the end of each pulse, the temperature of the sample increases from pulse to pulse, making possible the inversion of a larger region when the temperature overcomes T_C. That causes the expansion of the inverted domain with the number of pulses. With a high enough number of pulses, the heated area stops increasing due to the cooling though the substrate and no further increase of the inverted domain is obtained, in good accordance with the experiments (see, for instance, Fig. 4 in [7]). The temporal evolution of the averaged m_z component in a sample initially magnetized down is presented in Fig. 4. Starting from a value close to -0.9, indicating that the sample is initially magnetized down, with high enough values of the fluence, this value increases up to ~-0.7. As $<m_z>$ represents the average of m_z over the whole sample, the increase from -0.9 to -0.7 means that some part of the sample reach positive local values of m_z, corresponding to the central inverted region.

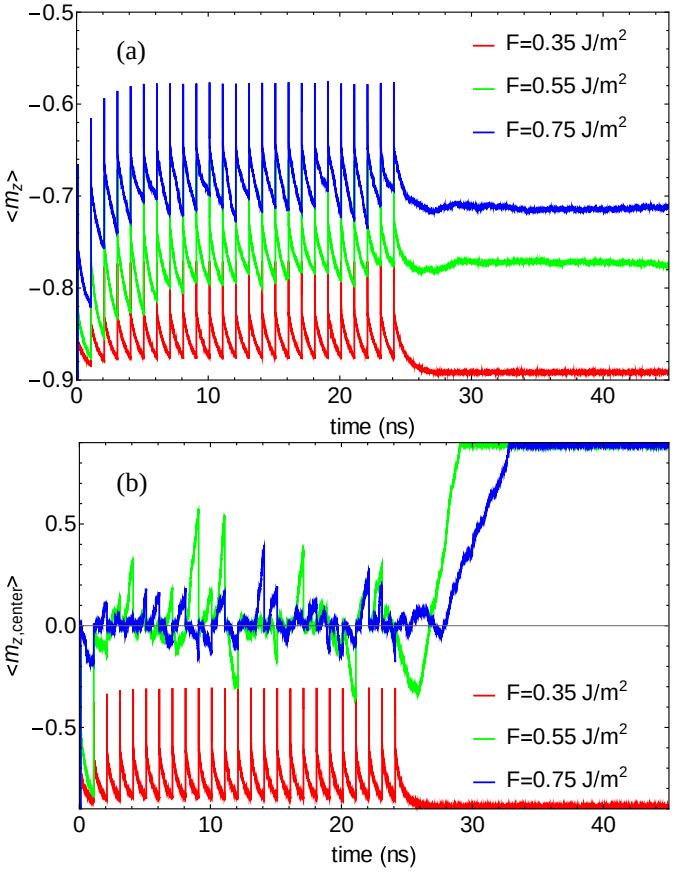

Fig. 4. (a) Time evolution of the averaged out-of-plane magnetization of a sample initially magnetized down ($<m_z>=-1$) as submitted to a train of 25 pulses with positive helicity (σ^+) for three different fluence values (F). (b) Temporal evolution of the magnetization averaged over a circular region of radius $r=100$ nm around the center of the sample, $<m_{z,center}>$ for the same fluences as in (a).

IV. Conclusion

An advanced micromagnetic model, which couples the magnetization dynamics to the temporal evolution of the temperature of the sample, and takes into account a helicity-dependent magneto-optical effective field, has been developed and used to describe experimental observations of the HD-AOS processes in ultra-thin ferromagnetic films with high perpendicular anisotropy. Micromagnetic simulations of the LLB equation combined with the 3TM and the IFE explains the observed behavior of recent AOS experiments. The existence of a fluence threshold and the increase of the inverted area with the number of pulsed is explained by the thermal activation caused by the laser heating and the nucleation of domains in one or the other orientation depending on the sign of the magneto-optical field created by the laser helicity. Our model constitutes a significant step towards a further understanding of the physics involved in these optically-induced processes. It will be useful to describe other experimental observations in ferromagnetic systems, and it can be naturally extended to describe the excitation of the magnetization by laser pulses in other systems such ferrimagnetic and antiferromagnetic systems. Moreover, it can

also be extended to include other physical mechanisms as the magnetic circular dichroism and/or the optical excitation of spin currents by laser pulses, which will allow us to evaluate the real scope of these mechanisms from a realistic point of view.

ACKNOWLEDGMENT

This work was supported by projects MAT2014- 52477-C5-4-P, MAT2017-87072-C4-1-P, and MAT2017-90771-REDT from the Spanish government, and projects SA090U16 and SA299P18 from the Junta de Castilla y Leon.

REFERENCES

[1] C. D. Stanciu et al., “All-optical magnetic recording with circularly polarized light”, Phys. Rev. Lett., vol. 99, no. 4, pp. 1–4, 2007.

[2] C. D. Stanciu et al., “Ultrafast spin dynamics across compensation points in ferrimagnetic GdFeCo: The role of angular momentum compensation”, Phys. Rev. B - Condens. Matter Mater. Phys., vol. 73, no. 22, pp. 1–4, 2006.

[3] U. Atxitia, T. Ostler, J. Barker, R. F. L. Evans, R. W. Chantrell, and O. Chubykalo-Fesenko, “Ultrafast dynamical path for the switching of a ferrimagnet after femtosecond heating”, Phys. Rev. B - Condens. Matter Mater. Phys., vol. 87, no. 22, pp. 1–5, 2013.

[4] M. L. M. Lalieu, M. J. G. Peeters, S. R. R. Haenen, R. Lavrijsen, and B. Koopmans, “Deterministic all-optical switching of synthetic ferrimagnets using single femtosecond laser pulses”, Phys. Rev. B, vol. 96, no. 22, pp. 1–5, 2017.

[5] C. H. Lambert et al., “All-optical control of ferromagnetic thin films and nanostructures”, Science (80-.)., vol. 345, no. 6202, pp. 1337–1340, 2014.

[6] M. S. El Hadri et al., “Two types of all-optical magnetization switching mechanisms using femtosecond laser pulses”, 2016.

[7] R. Medapalli et al., “Multiscale dynamics of helicity-dependent all-optical magnetization reversal in ferromagnetic Co/Pt multilayers”, Phys. Rev. B, vol. 96, no. 22, pp. 1–8, 2017.

[8] G. Malinowski et al., “Control of speed and efficiency of ultrafast demagnetization by direct transfer of spin angular momentum”, Nat. Phys., vol. 4, no. 11, pp. 855–858, 2008.

[9] B. Koopmans et al., “Explaining the paradoxical diversity of ultrafast laser-induced demagnetization,” Nat. Mater., vol. 9, no. 3, pp. 259–265, 2010.

[10] K. Vahaplar et al., “All-optical magnetization reversal by circularly polarized laser pulses: Experiment and multiscale modeling”, Phys. Rev. B, vol. 85, no. 10, p. 104402, 2012.

[11] S. Ali, J. R. Davies, and J. T. Mendonca, “Inverse faraday effect with linearly polarized laser pulses”, Phys. Rev. Lett., vol. 105, no. 3, pp. 1–4, 2010.

[12] R. Hertel, “Theory of the inverse Faraday effect in metals”, J. Magn. Magn. Mater., vol. 303, no. 1, pp. 1–4, 2006.

[13] K. Taguchi, J. I. Ohe, and G. Tatara, “Ultrafast magnetic vortex core switching driven by the topological inverse Faraday effect”, Phys. Rev. Lett., vol. 109, no. 12, pp. 1–5, 2012.

[14] A. Stupakiewicz, K. Szerenos, D. Afanasiev, A. Kirilyuk, and A. V. Kimel, “Ultrafast nonthermal photo-magnetic recording in a transparent medium”, Nature, vol. 542, no. 7639, pp. 71–74, 2017.

[15] I. Radu et al., “Transient ferromagnetic-like state mediating ultrafast reversal of antiferromagnetically coupled spins,” Nature, vol. 472, no. 7342, pp. 205–209, 2011.

[16] A. R. Khorsand et al., “Role of magnetic circular dichroism in all-optical magnetic recording,” Phys. Rev. Lett., vol. 108, no. 12, pp. 1–5, 2012.

[17] A. V. Kimel, A. Kirilyuk, A. Tsvetkov, R. V. Pisarev, and T. Rasing, “Laser-induced ultrafast spin reorientation in the antiferromagnet TmFeO3”, Nature, vol. 429, no. 6994, pp. 850–853, 2004.

[18] D. Rudolf et al., “Ultrafast magnetization enhancement in metallic multilayers driven by superdiffusive spin current,” Nat. Commun., vol. 3, pp. 1036–1037, 2012.

[19] I. Razdolski et al., “Nanoscale interface confinement of ultrafast spin transfer torque driving non-uniform spin dynamics”, Nat. Commun., vol. 8, pp. 1–5, 2017.

[20] A. J. Ramsay et al., “Optical spin-transfer-torque-driven domain-wall motion in a ferromagnetic semiconductor”, Phys. Rev. Lett., vol. 114, no. 6, pp. 1–5, 2015.

[21] G. M. Choi, A. Schleife, and D. G. Cahill, “Optical-helicity-driven magnetization dynamics in metallic ferromagnets”, Nat. Commun., vol. 8, pp. 1–7, 2017.

[22] T. D. Cornelissen, R. Córdoba, and B. Koopmans, “Microscopic model for all optical switching in ferromagnets Microscopic model for all optical switching in ferromagnets”, Appl. Phys. Lett., vol. 108, no. 2016, p. 142405, 2016.

[23] Z. Du, C. Chen, F. Cheng, Y. Liu, and L. Pan, “Prediction of deterministic all-optical switching of ferromagnetic thin film by ultrafast optothermal and optomagnetic couplings”, Sci. Rep., vol. 7, no. 1, pp. 1–12, 2017.

[24] R. F. L. Evans, D. Hinzke, U. Atxitia, U. Nowak, R. W. Chantrell, and O. Chubykalo-Fesenko, “Stochastic form of the Landau-Lifshitz-Bloch equation”, Phys. Rev. B - Condens. Matter Mater. Phys., vol. 85, no. 1, pp. 1–9, 2012.

[25] U. Atxitia, P. Nieves, and O. Chubykalo-Fesenko, “Landau-Lifshitz-Bloch equation for ferrimagnetic materials”, Phys. Rev. B - Condens. Matter Mater. Phys., vol. 86, no. 10, 2012.

[26] M. G. Haines, “Generation of an axial magnetic field from photon spin”, Phys. Rev. Lett., vol. 87, no. 13, pp. 1–4, 2001.

[27] R. Hertel, “Theory of the inverse Faraday effect in metals”, J. Magn. Magn. Mater., vol. 303, no. 1, 2006.

[28] P. Nieves and O. Chubykalo-Fesenko, “Modeling of Ultrafast Heat- and Field-Assisted Magnetization Dynamics in FePt”, Phys. Rev. Appl., vol. 5, no. 1, pp. 1–8, 2016.

[29] K. Vahaplar et al., “Ultrafast Path for Optical Magnetization Reversal via a Strongly Nonequilibrium State”, Phys. Rev. Lett., vol. 103, no. 11, pp. 66–69, 2009.

[30] S. Moretti, V. Raposo, and E. Martinez, “Influence of Joule heating on current-induced domain wall depinning”, J. Appl. Phys., vol. 119, no. 21, p. 213902, 2016.

[31] V. Raposo, S. Moretti, M. A. Hernandez, and E. Martinez, "Domain wall dynamics along curved strips under current pulses: The influence of Joule heating", Appl. Phys. Lett. vol 108, p. 042405, 2016

[32] E. Martínez, O. Alejos, M. A. Hernández, V. Raposo, L. Sánchez-Tejerina, and S. Moretti, "Angular dependence of current-driven chiral walls" Appl. Phys. Express vol.9, p. 063008 ,2016.